Journal of ELECTRONIC MATERIALS, Vol. 46, No. 5, 2017
DOI: 10.1007/s11664-016-5056-6

Thermoelectric Properties of $Mg_2Si_{0.995}Sb_{0.005}$ Prepared by the High-Pressure High-Temperature Method

JIALIANG LI,[1] GANG CHEN,[1,5] BO DUAN,[1] YAJU ZHU,[1] XIAOJUN HU,[2] PENGCHENG ZHAI,[1,3,6] and PENG LI[4]

1.—School of Science, Wuhan University of Technology, Wuhan, China. 2.—High Pressure High Temperature Institute of Physics, Wuhan University of Technology, Wuhan, China. 3.—State Key Laboratory of Advanced Technology for Materials Synthesis and Processing, Wuhan University of Technology, Wuhan, China. 4.—School of Mechanical and Electronic Engineering, Wuhan University of Technology, Wuhan, China. 5.—e-mail: cg_chen@whut.edu.cn. 6.—e-mail: pczhai@126.com

$Mg_2Si_{0.995}Sb_{0.005}$ compound was prepared by the high-pressure high-temperature (HPHT) method. The simultaneous synthesis and consolidation in one step could be completed in < 15 min. The effects of pressure and temperature on the thermoelectric properties of $Mg_2Si_{0.995}Sb_{0.005}$ were analyzed in this work. With the pressure and temperature increasing, the electrical conductivity rises markedly, while the Seebeck coefficient changes slightly, which results in significant enhancement of the power factor. The $Mg_2Si_{0.995}Sb_{0.005}$ sample prepared under the condition of 1073 K and 2 GPa achieves the highest power factor of $\sim 2.12 \times 10^{-3}$ W m^{-1} K^{-2} at 575 K. As the sample prepared at 973 K and 2 GPa retains a lower thermal conductivity, it obtains the highest thermoelectric figure-of-merit ZT ~0.62 at 800 K. In conclusion, the HPHT method can serve as a route to prepare Sb-doped Mg_2Si thermoelectric materials efficiently.

Key words: Mg_2Si, thermoelectric material, high-pressure high-temperature, thermoelectric properties

INTRODUCTION

Magnesium silicide (Mg_2Si)-based thermoelectric materials are promising candidates in the middle temperature range (500–800 K) for converting heat into electricity efficiently. The elements of Mg_2Si compounds are abundant in the Earth's crust, and low-cost and nontoxic, which are consistent with the policy for environmentally-friendly development. They have low density (< 2 g cm^{-3}) and high thermal stability (melting temperature ~1273 K), which encourages growth of the light and economical systems used in aerospace and military vehicles.[1] Although Mg_2Si is not as efficient as $Mg_2Si_{1-x}Sn_x$,[2,3] it also exhibits a promising thermoelectric performance due to its high carrier mobility, large effective mass and comparatively low lattice thermal conductivity.

Pressure can significantly modify the electron band structure and energy gap of thermoelectric materials.[4] For instance, both Bi_2Te_3 in ~5–7 GPa[5] and PbTe in ~13–16 GPa[6] demonstrate a metalization tendency, and that permitting modulation E_g and hence optimizing the thermoelectric state.[4] Mg_2Si is an indirect narrow band gap semiconductor and consists of an anti-fluorite crystal structure with Si in FCC (face-centered cubic) sites and Mg in tetrahedral positions. It has large interstitial voids in the center, suggesting that the lattice is rather soft, and thus may be significantly modified by applied pressure.[7] It has been established that Mg_2Si undergoes structural phase transition (cubic anti-fluorite structure, orthorhombic anti-cotunnite structure and hexagonal Ni_2In-type structure) under high pressure.[8–12] Recently, it was reported that the power factor of Al-doped Mg_2Si reaches the maximum value of about 8×10^{-3} W m^{-1} K^{-2} in the pressure range of 2–3 GPa in ambient conditions, which far outweighs its counterparts in the

(Received June 9, 2016; accepted October 11, 2016; published online October 26, 2016)

Table I. Physical parameters of all samples at room temperature

Sample no.	HPHT parameters	Density (g cm^{-3})	σ (10^4 × S m^{-1})	α (μ V K^{-1})	κ_L (W m^{-1} K^{-1})
1	973 K–2 GPa	2.02	1.09	−118.5	5.52
2	1023 K–2 GPa	2.02	4.80	−97.8	7.81
3	1023 K–2.5 GPa	2.03	5.20	−112.8	8.18
4	1073 K–2 GPa	2.02	6.15	−102.8	8.48
5	1123 K–2.5 GPa	2.03	6.24	−114.5	9.08

published literature.[7] However, the enhancement diminishes once the pressure is removed, indicating that the high-pressure processing in ambient conditions is reversible. Thus, the high-pressure high-temperature (HPHT) route has been employed for synthesizing thermoelectric materials aiming to achieve the above superior thermoelectric properties at high pressure. Some traditional thermoelectric materials like PbTe, $AgSbTe_2$, $CoSb_3$ prepared by the HPHT route also show improved thermoelectric properties and high efficiency.[13–15] Up to now, there has been no report of Sb-doped Mg_2Si prepared by the HPHT route. This work is focusing on the HPHT processing of $Mg_2Si_{0.995}Sb_{0.005}$ and establishing its thermoelectric properties.

EXPERIMENTAL

High-purity powders of Mg (99.5%), Si (99.99%) and Sb (99.999%) in stoichiometric ratio, dipped in hexane, were well mixed in an agate mortar and then pressed into pellets of 3 mm in height and 15.2 mm in diameter. The bulk of the $Mg_2Si_{0.995}Sb_{0.005}$ compound was prepared by the HPHT method in one step on a cubic multi-anvil apparatus. The simultaneous synthesis and consolidation of $Mg_2Si_{0.995}Sb_{0.005}$ in one step were completed at the pressure of 2–2.5 GPa and the temperature of 973–1123 K within 15 min.

The constituent phases were measured by x-ray diffraction (XRD; Bruker: D8 Advance, CuKα). The samples' micro-structures were characterized by using field emitting scanning electron microscopy (FESEM; Zeiss Ultra plus). The back-scattered electron images (BSI) and the chemical composition of the polished surfaces were obtained with an electron probe micro-analyzer (EPMA; JXA-8230, Japan) equipped with wavelength dispersive x-ray spectroscopy (WDS). The electrical conductivity and the Seebeck coefficient were measured simultaneously by the standard four-probe method (ZEM-3; Sinku-riko) in a He atmosphere. The thermal conductivity was calculated from the measured thermal diffusivity (λ), heat capacity (C_p), and density (d) by the equation: $\kappa = C_p\lambda d$. d and λ were measured by the Archimedes method and laser-flash technique (Netzsch: LFA 457), and C_p refers to the data from NIST (National Institute of Standards and Technology). The uncertainties are ±5% for the electrical conductivity and the Seebeck coefficient, and ±7% for the thermal conductivity, leading to ~10% uncertainty in ZT.

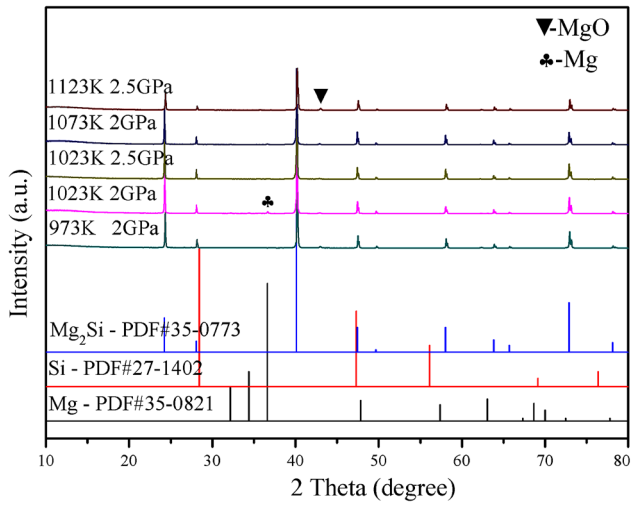

Fig. 1. The XRD patterns of $Mg_2Si_{0.995}Sb_{0.005}$ prepared by HPHT.

RESULTS AND DISCUSSION

Table I shows some room-temperature physical parameters for all samples. The XRD patterns in Fig. 1 show that all the compounds prepared by the HPHT are almost single phase materials. Tiny Mg and MgO peaks are detected in almost all samples which is common in synthesized Mg_2Si compounds.[16–20] The impurity becomes even weaker when the pressure grows to 0.5 GPa higher or the temperature goes 50 K higher. The main Bragg peaks perfectly match the standard peaks of Mg_2Si (PDF#035-0773) which crystallizes into the cubic anti-fluorite structure. This indicates that the HPHT method is applicable to the synthesis of Mg_2Si-based thermoelectric materials.

Figure 2 shows the micrographs of the fresh fracture surface obtained by FESEM. It is clear that the matrix is densely compacted, which is in agreement with the high density values as shown in Table I. The grain size of the matrix is about 2–6 μm as shown in Fig. 2a and b. This demonstrates that dense $Mg_2Si_{0.995}Sb_{0.005}$ bulks can be obtained through the HPHT route in one step. Figure 3a manifests the back-scattered electron images (BSI) of the polished surface of the sample under the conditions of 1023 K and 2 GPa, and reveals that

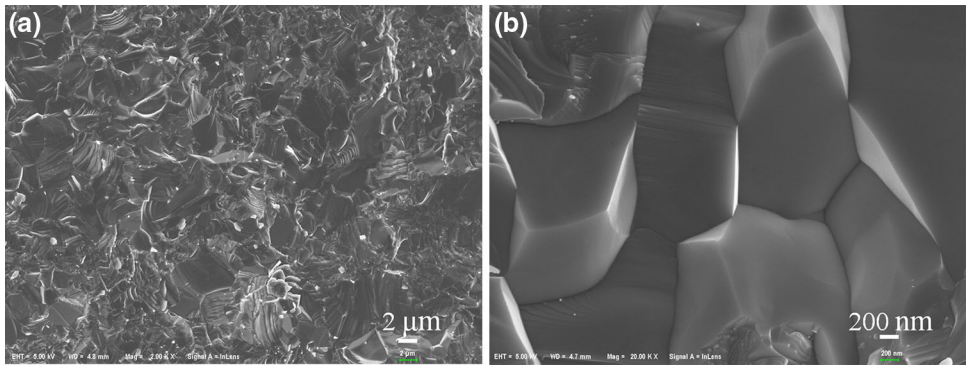

Fig. 2. The different magnified micro-graph of the fresh fracture surfaces of sample under 1073 K–2 GPa, (a) ×2000, (b) ×20,000.

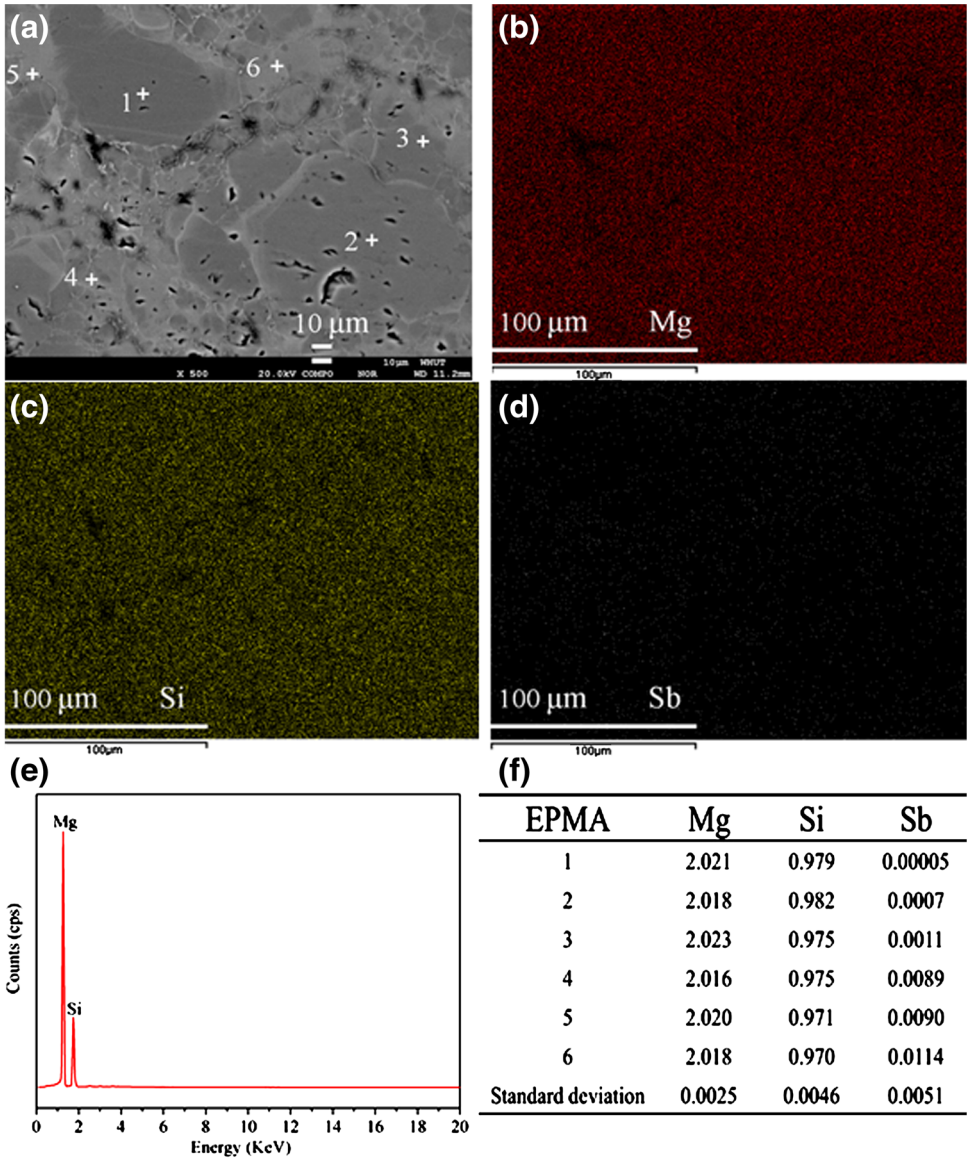

(f)

EPMA	Mg	Si	Sb
1	2.021	0.979	0.00005
2	2.018	0.982	0.0007
3	2.023	0.975	0.0011
4	2.016	0.975	0.0089
5	2.020	0.971	0.0090
6	2.018	0.970	0.0114
Standard deviation	0.0025	0.0046	0.0051

Fig. 3. Sample under 1073 K–2 GPa: (a) BSI on polished surface; (b, c) Mg, Si, Sb elements distribution maps; (d) EDS on FESEM; (e) WDS on EPMA.

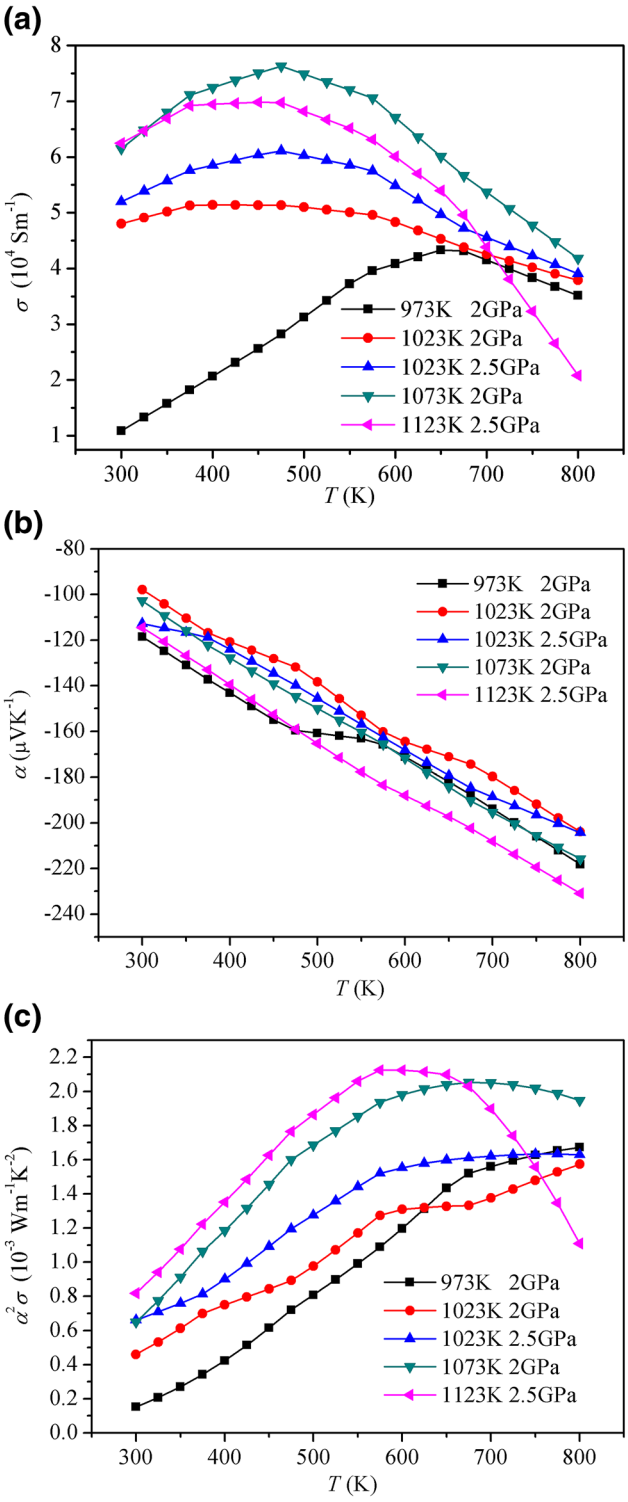

Fig. 4. The temperature-dependent electrical conductivity (a), Seebeck coefficient (b), and power factor (c) of all samples.

there is phase segregation in the specimen, whose scenario is similar to those of samples prepared by the self-propagating high-temperature synthesis method.[21] Together with the elemental distribution maps (Fig. 3b–d), it is proved that Mg and Si are distributed evenly on the micro-scale, but Sb is not. However, Sb is not reflected by the energy dispersive spectrum (EDS) as shown in Fig. 3e due to its trace amount. Actually, the varied contents of Sb in different areas are determined by using the EPMA with WDS, which are listed in Fig. 3f. It can be inferred that the Sb content in the bright gray areas is significantly larger than in the dark gray areas.

Temperature-dependent electronic transport properties are shown in Fig. 4. It is identified that Sb occupies the Si site acting as a donor to effectively enhance the electron carrier concentration.[22,23] The electrical conductivity of Sb-doped Mg_2Si is significantly enhanced compared to that of pure Mg_2Si.[24] While the temperature and pressure increase, the highest value of the electrical conductivity for the sample prepared under 1023 K and 2 GPa is 7.6×10^5 S m^{-1}. As the pressure and temperature reach 2.5 GPa and 1123 K, the sample's electrical conductivity is weakened slightly. With temperature increasing gradually, the electrical conductivity firstly increases, then drops. In the low temperature range, the intrinsic excitation may happen which results in more electron carriers and thus increases the electrical conductivity,[25,26] while in the high temperature range, the temperature dependence of mobility follows $\mu \propto T^{-3/2}$ and the acoustic lattice scattering becomes the predominant mechanism.[25–27] Thus, the electrical conductivity drops rapidly in high temperature ranges. The absolute values of the Seebeck coefficient increase roughly monotonously with temperature. Since all samples have the same nominal composition and similar carrier concentrations, the Seebeck coefficients approximately approach each other.

Experiencing compensation between electrical conductivity and Seebeck coefficient, the power factor is marginally enhanced for the samples under the conditions of 1023 K–2 GPa and 1123 K–2.5 GPa, and both reach the maximum value of 2.1×10^{-3} W m^{-1} K^{-2}.

Figure 5 displays the temperature-dependent thermal conductivity κ. It is obvious that the κ of the sample under the condition of 973 K–2 GPa is the lowest compared to others in the whole temperature range. The κ of the other samples demonstrate little deviation, especially at 600–800 K. At 300–600 K, the thermal conductivity rises a little with the increasing pressure and temperature. The lattice thermal conductivity κ_L is presented in the inset of Fig. 5. The term κ_L is obtained from the total thermal conductivity κ by subtracting the electronic thermal conductivity $L\sigma T$ (using the Wiedemann–Franz law) where L is the Lorentz number (2.45×10^{-8} V^2 K^{-2}).[28,29] It is obvious that κ_L dominates the thermal conductivity for all samples and the κ_L of samples prepared by the HPHT method is much lower than by other routes.[21]

In general, κ_L is described by the equation $\kappa_L = (1/3)C_v v l = (1/3)C_v v^2 \tau$., where C_v, v, l, τ are the specific

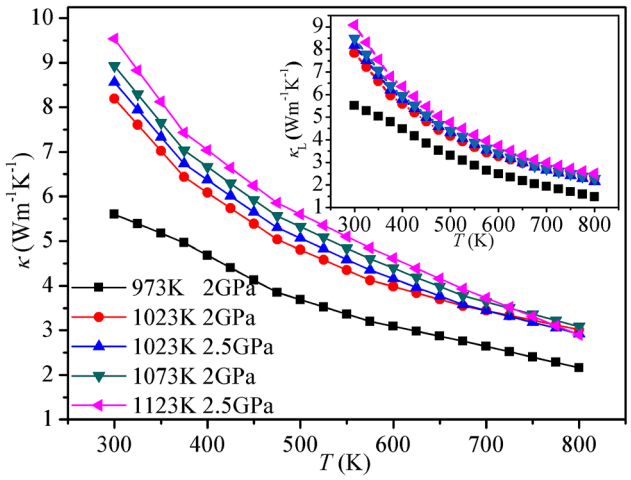

Fig. 5. The temperature-dependent thermal conductivity and lattice thermal conductivity (inset).

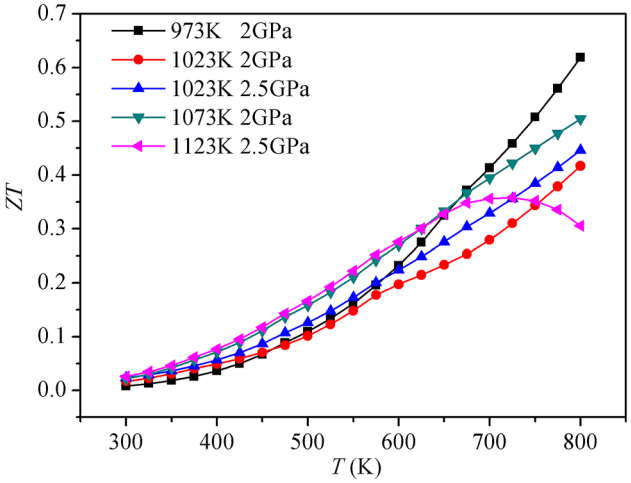

Fig. 6. The temperature-dependent dimensionless thermoelecric figure of merit, *ZT*.

heat, phonons velocity, phonons mean free path and phonons relaxation time, respectively. The overall relaxation time is expressed as $1/\tau = 1/\tau_B + 1/\tau_D + 1/\tau_U$ where τ_B, τ_D and τ_U represent phonons relaxation time concerning grain boundary scattering, point defect scattering and phonon–phonon U-process scattering. High-frequency phonons can be effectively impeded by point defect scattering such as Sb doping and residual strain. The mass and radius of Sb and Si atoms differ greatly which results in mass fluctuation and strain. Meanwhile, the compression of the Mg-Si bonds introduced by the HPHT could cause a slight change in the lattice vibration mode. Those factors will result in strong phonons scattering and consequently decrease the lattice thermal conductivity.

The temperature dependence of the *ZT* for $Mg_2Si_{0.995}Si_{0.005}$ compounds calculated from the above data is presented in Fig. 6. Except for the sample under 1123 K–2.5 GPa, as the temperature increases, the *ZT* values increase monotonously. The maximum value of 0.62 is achieved at 800 K for the compound prepared under 973 K and 2 GPa, which is comparable to the results in the published literature.[21,22,26]

CONCLUSIONS

The $Mg_2Si_{0.995}Sb_{0.005}$ bulks were prepared by the HPHT route within 15 min, which merged the synthesis and the consolidation into one step. The phase and micro-structure have been evaluated carefully and the data indicate that Sb is not distributed evenly. With pressure and temperature rising, the electrical conductivity is significantly enhanced. The absolute values of the Seebeck coefficients are increasing monotonously and the power factors reach the maximum values of 2.1×10^{-3} W m^{-1} K^{-2} for the samples prepared under 1073 K–2 GPa and 1123 K–2.5 GPa. The lattice thermal conductivity dominates the thermal transport and decreases rapidly with temperature. Due to the point defect scattering introduced by the Sb dopants and high pressure, κ_L is lower than most results in the literature. As a result, the maximum thermoelectric dimensionless figure of merit *ZT* ~0.62 is achieved at 800 K. This indicates that HPHT is an effective route for preparing Sb-doped Mg_2Si thermoelectric materials.

ACKNOWLEDGEMENTS

This work was supported by the National Natural Science Foundation of China (No. 51272198), the National Basic Research Program of China (No. 2013CB632505), the International S&T Cooperation Program of China (2014DFA63070), and the Fundamental Research Funds for the Central Universities (No. 2016IB001). Besides, J.L. Li is grateful to C.H. Shen and M.J. Yang for their help with XRD and EPMA in Materials Research and Test Center of WUT.

REFERENCES

1. M. Ioannou, K. Chrissafis, E. Pavlidou, F. Gascoin, and T. Kyratsi, *J. Solid State Chem.* 197, 172 (2013).
2. W. Liu, X. Tang, H. Li, K. Yin, J. Sharp, X. Zhou, and C. Uher, *J. Mater. Chem.* 22, 13653 (2012).
3. W. Liu, Q. Zhang, K. Yin, H. Chi, X. Zhou, X. Tang, and C. Uher, *J. Solid State Chem.* 203, 333 (2013).
4. S.V. Ovsyannikov and V.V. Shchennikov, *Chem. Mater.* 22, 635 (2010).
5. S.V. Ovsyannikov, V.V. Shchennikov, G.V. Vorontsov, A.Y. Manakov, A.Y. Likhacheva, and V.A. Kulbachinskii, *J. Appl. Phys.* 104, 053713 (2008).
6. V. Shchennikov and S. Ovsyannikov, *Solid State Commun.* 126, 373 (2003).
7. N. Morozova, S. Ovsyannikov, I. Korobeinikov, A. Karkin, K. Takarabe, Y. Mori, S. Nakamura, and V. Shchennikov, *J. Appl. Phys.* 115, 213705 (2014).
8. J. Zhao, Z. Liu, R.A. Gordon, K. Takarabe, J. Reid, and J.S. Tse, *J. Appl. Phys.* 118, 145902 (2015).
9. W. Ren, Y. Han, C. Liu, N. Su, Y. Li, B. Ma, Y. Ma, and C. Gao, *Solid State Commun.* 152, 440 (2012).
10. F. Yu, J. Sun, W. Yang, R. Tian, and G. Ji, *Solid State Commun.* 150, 620 (2010).

11. J. Hao, Z. Guo, and Q. Jin, *Solid State Commun.* 150, 2299 (2010).
12. J. Hao, B. Zou, P. Zhu, C. Gao, Y. Li, D. Liu, K. Wang, W. Lei, Q. Cui, and G. Zou, *Solid State Commun.* 149, 689 (2009).
13. P. Zhu, X. Jia, H. Chen, W. Guo, L. Chen, D. Li, H. Ma, G. Ren, and G. Zou, *Solid State Commun.* 123, 43 (2002).
14. T. Su, X. Jia, H. Ma, C. Zang, L. Zhou, J. Guo, and N. Dong, *Mater. Lett.* 62, 3269 (2008).
15. L. Deng, H. Ma, T. Su, F. Yu, Y. Tian, Y. Jiang, N. Dong, S. Zheng, and X. Jia, *Mater. Lett.* 63, 2139 (2009).
16. S. Fiameni, A. Famengo, F. Agresti, S. Boldrini, S. Battiston, M. Saleemi, M. Johnsson, M.S. Toprak, and M. Fabrizio, *J. Electron. Mater.* 43, 2301 (2014).
17. J. de Boor, C. Compere, T. Dasgupta, C. Stiewe, H. Kolb, A. Schmitz, and E. Mueller, *J. Mater. Sci.* 49, 3196 (2014).
18. J. Tani and H. Kido, *Intermetallics* 32, 72 (2013).
19. M. Saleemi, M.S. Toprak, S. Fiameni, S. Boldrini, S. Battiston, A. Famengo, M. Stingaciu, M. Johnsson, and M. Muhammed, *J. Mater. Sci.* 48, 1940 (2012).
20. M. Ioannou, E. Hatzikraniotis, C. Lioutas, T. Hassapis, T. Altantzis, K.M. Paraskevopoulos, and T. Kyratsi, *Powder Technol.* 217, 523 (2012).
21. Q. Zhang, X. Su, Y. Yan, H. Xie, T. Liang, Y. You, X. Tang, and C. Uher, *ACS Appl. Mater. Interfaces* 8, 3268 (2016).
22. N. Farahi, M. VanZant, J. Zhao, J. Tse, S. Prabhudev, G. Botton, J. Salvador, F. Borondics, Z. Liu, and H. Kleinke, *Dalton Trans.* 43, 14983 (2014).
23. P. Zwolenski, J. Tobola, and S. Kaprzyk, *J. Electron. Mater.* 40, 889 (2011).
24. J. Jung and I. Kim, *Electron. Mater. Lett.* 6, 187 (2010).
25. J. Tani and H. Kido, *Phys. B Condens. Matter.* 364, 218 (2005).
26. J. Tani and H. Kido, *Intermetallics* 15, 1202 (2007).
27. R. LaBotz, D. Mason, and D. O'Kane, *J. Electrochem. Soc.* 110, 127 (1963).
28. X. Lin, D. Wang, M. Beekman, and G. Nolas, *Mater. Res. Soc.* 1044, 155 (2008).
29. T. Dasgupta, C. Stiewe, R. Hassdorf, A.J. Zhou, L. Boettcher, and E. Mueller, *Phys. Rev. B* 83, 235207 (2011).